Energy Engineering

Tech Science Press

Doi:10.32604/ee.2025.073787

ARTICLE

Optimal Allocation of Distributed Generation and Energy Storage Considering Line Vulnerability under Extreme Weather in Distribution Networks

Yangjun Zhou[1], Chenying Yi[1], Wei Zhang[1], Juntao Pan[2,*], Ke Zhou[1], Weixiang Huang[1], Like Gao[1], Shan Li[1], Yuanchao Zhou[3], Ling Li[2], Liwen Qin[1], Hongwen Wu[4] and Lijuan Yan[2]

[1]Guangxi Key Laboratory of Intelligent Control and Maintenance of Power Equipment, Electric Power Research Institute of Guangxi Power Grid Co., Ltd., Nanning, 530000, China
[2]Guangxi Power Grid Co., Ltd., Nanning, 530000, China
[3]Nanning Power Supply Bureau, Guangxi Power Grid Co., Ltd., Nanning, 530031, China
[4]Wuzhou Power Supply Bureau, Guangxi Power Grid Co., Ltd., Wuzhou, 543002, China

*Corresponding Author: Juntao Pan. Email: pan_jt.sy@gx.csg.cn

Received: 25 September 2025; Accepted: 20 November 2025; Published: 27 May 2026

ABSTRACT: The increasing integration of distributed generation (DG) and energy storage systems (ESS) has significantly enhanced the flexibility and efficiency of distribution networks. However, the growing frequency of extreme weather events has exposed the vulnerability of distribution lines, posing serious challenges to the reliability and resilience of such systems. Existing DG and ESS planning models often neglect this vulnerability dimension, leading to suboptimal siting decisions and reduced system robustness. To address this issue, this paper proposes a comprehensive multi-objective optimization framework that coordinates the allocation of DG and ESS and explicitly incorporates line vulnerability under extreme weather conditions. The vulnerability index of each distribution line is first evaluated through Monte Carlo simulations that capture the probabilistic influence of micro-climatic and terrain factors. This assessment serves as a pre-processing stage that screens out high-risk lines and thereby constrains the optimization decision space to more reliable nodes for DG and ESS deployment. Building upon this filtered network, a multi-objective optimization model is established to determine the optimal siting and capacities of DG and ESS. The optimization simultaneously minimizes the total annual cost, which includes investment, operation, and maintenance expenses, as well as network power losses, while improving overall system resilience. A case study on a modified IEEE 33-bus distribution system verifies the effectiveness of the proposed method. The results demonstrate that vulnerability-aware planning achieves a better balance between cost and reliability compared with conventional approaches. Specifically, the proposed strategy reduces annual network losses and outage durations while maintaining voltage stability with respect to climate-adjusted line failure rates. Furthermore, the integration of ESS enables effective peak shaving and valley filling, improving system efficiency and operational flexibility. These findings confirm that incorporating line vulnerability into DG and ESS planning provides a practical and scalable pathway for enhancing the resilience and economy of distribution networks.

KEYWORDS: Distributed generation; energy storage systems; distribution networks; extreme weather; line vulnerability; multi-objective optimization

1 Introduction

With the continuous growth of global electricity demand, the development and integration of distributed generation (DG) technologies have accelerated significantly due to their clean and sustainable

Copyright © 2026 The Authors. Published by Tech Science Press.
This work is licensed under a Creative Commons Attribution 4.0 International License, which permits unrestricted use, distribution, and reproduction in any medium, provided the original work is properly cited.

nature. These technologies are not only critical to meeting increasing energy needs but also play a pivotal role in the ongoing transformation of the global energy structure [1–3]. In response to this transition, the optimal planning of DG in distribution networks has emerged as a central research topic. Various methods have been proposed for determining installation locations and capacity allocations. For instance, bi-level optimization models have been developed to address the output instability of DG [4]; deterministic transformation techniques have been applied to simplify stochastic problems caused by DG uncertainty [5]; and multi-level coordinated planning strategies have been introduced to enhance allocation efficiency of DG in active distribution networks [6].

Nevertheless, large-scale DG integration has introduced operational challenges, particularly the temporal mismatch between generation and load demand. This mismatch often leads to wind and solar curtailment as well as load shedding, limiting the flexibility and reliability of distribution network operation [7]. To mitigate these issues, flexible technologies such as energy storage systems (ESS) and soft open points (SOPs) have been increasingly deployed. These technologies alleviate source-load imbalances, improve network adaptability, and enhance the overall stability and reliability of distribution systems [8].

The coordinated planning of DG and ESS not only facilitates the effective utilization of surplus renewable energy and reduces curtailment, but also enables stored energy to be dispatched during peak demand periods. This coordination helps mitigate the impact of DG uncertainty, balance system loads, and enhance operational stability [9]. Proper ESS sizing is particularly important: undersized ESS may result in underutilization of renewable resources and energy waste, while oversized systems can increase costs, reduce the charging efficiency, and shorten cycle life [10].

Accordingly, joint optimization of DG and ESS typically pursues two objectives: minimizing system cost and improving stability through ESS utilization. In [11], a predictive control strategy was developed to leverage forecast data, thereby improving ESS performance and reducing required capacity. A probabilistic approach was employed in [12] to determine optimal hybrid ESS capacity, with supercapacitors addressing fast power fluctuations and batteries handling energy storage, validated using real wind data. In [13], the coordinated operation of ESS and wind farms was shown to significantly extend ESS service life. A virtual ESS model combining offshore wind and tidal current energy was proposed in [14] to enhance distribution network planning, while ref. [15] developed a configuration strategy to facilitate wind power integration and reduce costs through strategic ESS regulation. Furthermore, a two-stage robust planning model was introduced in [16] to address wind power uncertainty and optimize ESS allocation.

Despite these advances, most existing studies primarily focus on economic optimization and operational coordination, while the potential of ESS and DG in enhancing the resilience of distribution networks under extreme weather conditions has received limited attention. In practical distribution systems, increasing climate uncertainty, including lightning, icing, and windstorms, can cause severe damage to vulnerable distribution lines, resulting in cascading failures and prolonged outages. However, current siting strategies of DG and ESS often rely mainly on network topology and load distribution, without considering the spatial and environmental vulnerability of power lines. This limitation reduces the effectiveness of DG and ESS planning in ensuring network reliability and resilience [17–19].

To address these limitations, this paper proposes a configuration optimization model for DG and ESS that incorporates line vulnerability under extreme weather conditions. A Monte Carlo–based analysis method is employed to evaluate line vulnerability considering micro-terrain and micro-climate characteristics. The resulting vulnerability indices are then integrated into a multi-objective optimization model to determine the optimal siting and capacities of DG and ESS. The proposed framework aims to improve distribution network stability and resilience while maintaining economic efficiency and ensuring reliable operation under adverse weather conditions.

2 Vulnerability Analysis of Power Lines in Distribution Networks

With the continuous advancement of renewable energy technologies, DG has been widely integrated into distribution networks, increasing system complexity. Lightning strikes, as a frequent extreme weather event, can cause severe damage to both power lines and DG units, particularly in areas with complex terrain and unstable atmospheric conditions. This section first introduces the classification of climate and terrain types relevant to lightning risk. A Monte Carlo method is then employed to sample micro-climate, terrain, and line fault conditions to assess the vulnerability of distribution lines. The results of the line vulnerability analysis will inform the selection of optimal DG installation locations in the following sections.

2.1 Climate and Terrain Typologies Relevant to Lightning Hazards

Among various natural disasters, lightning strikes occur frequently and pose a significant threat to overhead distribution lines, particularly in regions with complex terrain and volatile weather conditions. Given their high frequency and severe impact on the operational reliability of distribution networks, this study focuses specifically on lightning hazards as the primary type of extreme weather under consideration.

To effectively assess the risk of lightning hazards, this study considers two critical environmental factors: climate conditions and terrain types.

Based on long-term meteorological observations, the climate is classified into three representative states: rain/snow, cloudy, and sunny. The occurrence of lightning hazards is closely related to climate conditions. For example, rain and snow are typically accompanied by high humidity and atmospheric instability, which increase the likelihood of thunderstorms. Cloudy weather often indicates the onset of convective activity and is also associated with a higher risk of lightning. In contrast, sunny conditions are generally more stable, resulting in a lower probability of lightning strikes.

Likewise, the terrain along distribution lines is divided into four types: flatlands, hills, mountains, and highlands. Terrain characteristics not only shape local atmospheric dynamics—such as humidity levels and wind patterns—but also affect the exposure of power lines to lightning. For example, areas with higher elevation or rugged topography are more prone to lightning activity.

2.2 Line Fault Modeling under Extreme Weather Conditions

Given the memoryless property of distribution lines in operation, the number of faults k occurring within a unit period of time can be modeled using a Poisson distribution, expressed as:

$$p\left(X=k\right)=\frac{\lambda^{k}}{k!}e^{-\lambda} \tag{1}$$

where X is a discrete random variable representing the number of failures of a distribution line within a unit time, $X=k$ denotes the event that exactly k failures occur during that period, and λ is the average line failure rate per unit time.

Considering the vulnerability of distribution lines to extreme weather conditions, the line fault model is reformulated as:

$$p\left(X=k\right)=\frac{\left(\omega\lambda\right)^{k}}{k!}e^{-\omega\lambda} \tag{2}$$

where ω is the extreme weather impact factor and $\omega\lambda$ is the line failure rate per unit of time.

Then, the failure probability of a distribution line within a unit time can be defined as the probability that at least one failure occurs, which is given by:

$$p\left(X \neq 0\right) = 1 - p\left(X = 0\right) = 1 - e^{-\omega\lambda} \tag{3}$$

where $p\left(X = 0\right)$ represents the probability that no failure occurs during the time period.

2.3 Monte Carlo-Based Vulnerability Analysis Model for Power Lines

2.3.1 Sampling Analysis of Climate-Terrain Conditions in Distribution Networks

Based on the above analysis, three climatic conditions—rain and snow, cloudy, and sunny—and four terrain types—flatlands, mountains, hills, and highlands—are identified around the distribution network. Their combinations yield 12 distinct scenarios, as shown in Table 1 (terrain: 1-flatland, 2-mountain, 3-hill, 4-highland; climate: a-rain/snow, b-cloudy, c-sunny). The occurrence probability of each scenario is obtained from local meteorological data.

Table 1: Probability of 12 combinations of climate-terrain conditions in the distribution network area

State	Terrain	Climate	Probability
1	1	c	P_1
2	2	c	P_2
3	3	c	P_3
4	4	c	P_4
5	1	b	P_5
6	2	b	P_6
7	3	b	P_7
8	4	b	P_8
9	1	a	P_9
10	2	a	P_{10}
11	3	a	P_{11}
12	4	a	P_{12}

The sampling steps for determining the climate-terrain condition of the distribution network are as follows:

Step 1: Construct a discrete distribution function $F\left(x\right) = \sum_{i \leq x} P_i$ based on the probability of each combining climate-terrain condition;

Step 2: Run the rand function to generate a random number r between [0, 1], and when $F\left(i-1\right) < r < F\left(i\right)$ is satisfied, it can be determined that the current line is in the i-th combination state.

2.3.2 Vulnerability Evaluation of Distribution Lines under Lightning

Considering the radial structure, the distribution network can be regarded as a series connection of multiple line segments. Let X_i denote the proportion of all known lines that belong to segment i, and define its unavailability per line as U_i, as expressed in the following equation:

$$U_i = p_i X_i / \left(p_i X_i + \mu_i\right) \tag{4}$$

where p_i is the failure probability of i-th line under lightning disaster and can be calculated from (3), μ_i is the repair rate of i-th line, which is inversely related to repair time r_i.

It is worth noting that in (3), ω represents the probability of lightning disasters under different climate-terrain combinations, which can be obtained from meteorological statistics.

The pseudocode of the line vulnerability analysis model based on Monte Carlo random sampling is presented in Table 2.

Table 2: Pseudocode of the line vulnerability analysis model using Monte Carlo random sampling

01:	Read meteorological statistical data and transmission line data;
02:	Initialize the number of sampling trials $k = 1$ and set the total number of sampling trials M;
03:	Construct the discrete distribution function $F(x)$, with the combined state denoted as W;
04:	Initialize the line fault matrix $D = \{d_1, d_2, \ldots, d_i, \ldots\}$;
05:	Use the rand function to generate a random number r between $[0, 1]$;
06:	**If** $F(j-1) < r < F(j)$
07:	$W = j$;
08:	**End if**
09:	Return the combined state W;
10:	Calculate the unavailability of i-th line U_i based on Eq. (4);
11:	**If** $v \leq U_i$;
12:	Identify the loads affected by the failure of i-th line based on the distribution network topology, and denote the total affected load power as S_L;
13:	$d_i = d_i + S_L$;
14:	**If** $k > M$
15:	Return the matrix $D = \{d_1, d_2, \ldots, d_i, \ldots\}$;
16:	**Else** $k = k + 1$
17:	Return to Step 05;
18:	**End if**
19:	**Else** $i = i + 1$
20:	Return to Step 10;
21:	**End if**
22:	Normalize all elements in the line fault matrix D using the Min-Max normalization method and obtain the line vulnerability matrix $V = \{v_1, v_2, \ldots, v_i, \ldots\}$

As shown in Table 2, the vulnerability index quantitatively reflects both the probability of line failure and the severity of its consequences under lightning conditions. A higher vulnerability value indicates that a line is more likely to experience lightning-induced outages and will interrupt a larger number of downstream loads when a fault occurs.

2.3.3 Contribution of Vulnerability Evaluation to DG and ESS Planning

In practical distribution networks, the vulnerability of lines under lightning conditions can be effectively evaluated by collecting commonly available engineering data, including lightning activity statistics from

meteorological agencies, geographic and environmental attributes from GIS systems, network topology and load connection information from distribution management systems, as well as historical outage and maintenance records. Based on the Monte Carlo simulation and impact quantification approach introduced above, these datasets allow utilities to assess line vulnerability.

The proposed vulnerability index directly supports decision-making in distribution network planning by identifying low-risk lines and defining feasible candidate locations for DG and ESS integration. By filtering out high-risk lines and retaining only low-vulnerability locations as feasible installation candidates, the evaluation directly reduces the decision space and ensures that DG and ESS are deployed in more reliable areas. This enables the optimization model to operate more efficiently and with stronger practicality in real distribution network planning scenarios.

3 Optimal Configuration Model for DG and ESS

After calculating the vulnerability index of each line, nodes connected to lines with lower vulnerability are selected as candidate locations. An optimization model is then formulated to determine the optimal installation locations and capacities of DG and ESS.

3.1 Framework of the Optimal Configuration Model

The overall framework of the optimal configuration model for DG and ESS is shown in Fig. 1. First, a comprehensive line vulnerability analysis model is employed to identify lines with lower failure probability, which are used to determine candidate access locations for DG and ESS. Then, an optimization model is formulated to minimize the annual total cost and network losses, subject to constraints including power flow, node voltage, branch current, and the operational limits of ESS and SOP. The CPLEX solver is used to obtain the optimal installation locations and capacities of DG and ESS.

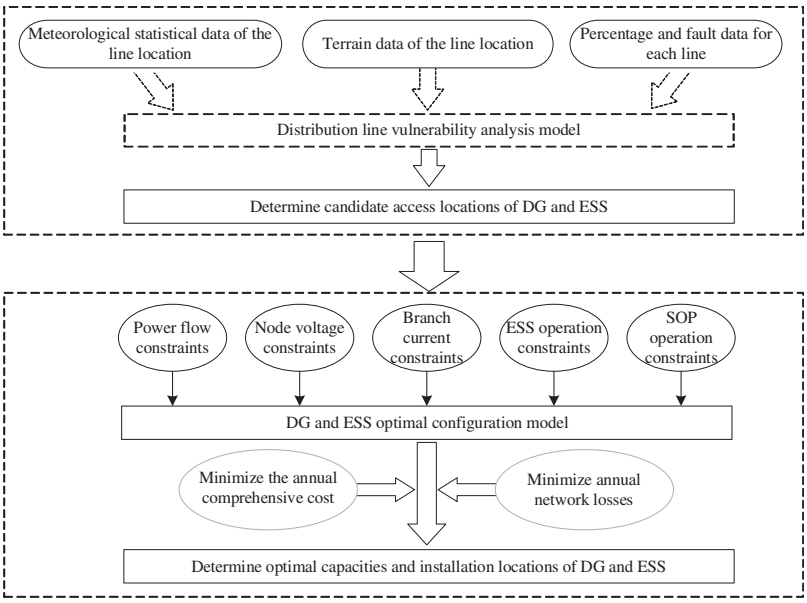

Figure 1: Overall framework of the optimal configuration model for DG and ESS

3.2 Objective Function

The DG and ESS planning model proposed in this paper is formulated as a multi-objective mixed-integer optimization problem. While heuristic algorithms are commonly used to solve such problems and obtain a Pareto-optimal solution set [20], they often suffer from slow convergence and sensitivity to initial conditions. To improve computational efficiency, this study adopts a linear weighting approach to transform the multi-objective problem into a single-objective optimization problem, which can be effectively solved using a commercial solver.

The objective function combines two key indices: the annual comprehensive cost and the annual network losses. Specifically, the annual comprehensive cost includes the investment and operation costs of DG and ESS, the electricity purchase cost from the main grid, and the cost associated with carbon emissions. This modeling approach ensures both economic efficiency and network performance in the planning of DG and ESS installations.

The objective function can be represented as:

$$f = \min \omega_1 \times \left(C_{\mathrm{DG}} + C_{\mathrm{ESS}} + C_{\mathrm{Buy}} + C_{\mathrm{CO_2}}\right) + \omega_2 \times F_{\mathrm{loss}} \tag{5}$$

where C_{DG} is the annual investment and operating costs of DG; C_{ESS} is the annual investment and operating costs of ESS; C_{Buy} is the cost of purchasing power from the main grid; $C_{\mathrm{CO_2}}$ is the cost of carbon emissions; F_{loss} is the annual network losses. ω_1 and ω_2 are weighting factors that balance the relative importance between the economic objective and the technical objective of network loss minimization. In this study, both investment and operating costs and annual network losses are considered equally important, and their magnitudes are on a similar scale, so the weights are set to $\omega_1 = 0.5$ and $\omega_2 = 0.5$.

The expression of C_{DG} is as follows:

$$C_{\mathrm{DG}} = \sum_{j \in N_{\mathrm{can}}} \gamma_j S_{\mathrm{DG},j} \left[\frac{r(r+1)^n}{(r+1)^n - 1} \times C_{\mathrm{inv},j} + C_{\mathrm{ope},j}\right] \tag{6}$$

where N_{can} is the set of nodes that are candidates for installation of distributed generation; γ_j denotes whether distributed generation is installed at node j; $S_{\mathrm{DG},j}$ is the capacity of distributed generation installed at node j; r is the fixed annual interest rate; n is the planning horizon; $C_{\mathrm{inv},j}$ is the investment cost per unit of capacity of distributed generation installed at node j; and $C_{\mathrm{ope},j}$ is the operating cost per unit of capacity of distributed generation installed at node j.

The expression of C_{ESS} is as follows:

$$C_{\mathrm{ESS}} = \sum_{i \in N_{\mathrm{can}}} v_i P_{\mathrm{ESS},i} \left[\frac{r(r+1)^n}{(r+1)^n - 1} \times C_{\mathrm{P},i} + C_{\mathrm{E},i}\right] \tag{7}$$

where N_{can} is the set of candidate nodes for ESS installation; v_i denotes whether ESS is installed at node i; $P_{\mathrm{ESS},i}$ is the installed capacity of ESS at node i; r is the fixed annual interest rate; n is the planning horizon; $C_{\mathrm{P},i}$ is the unit investment cost of ESS at node i; and $C_{\mathrm{E},i}$ is the unit operating cost of ESS at node i.

The expression of C_{Buy} is as follows:

$$C_{\mathrm{Buy}} = 365 \times \sum_{t=1}^{24} C_{\mathrm{b},t} \left(P_{\mathrm{load},t} - P_{\mathrm{DG},t} - P_{\mathrm{ESS},t}\right) \Delta t \tag{8}$$

where $C_{b,t}$ is the real-time electricity purchase price from the grid at time t; $P_{load,t}$ is the total active power demand of all load points at time t; $P_{DG,t}$ is the total active power output of all DG units at time t; and $P_{ESS,t}$ is the total active power output of all ESS units at time t.

The expression of C_{CO_2} is as follows:

$$C_{CO_2} = \frac{365 \times m \times e}{1000} \times \sum_{t=1}^{24} \left(P_{load,t} + P_{loss,t} - P_{DG,t} - P_{ESS,t}\right) \Delta t \tag{9}$$

where m the environmental penalty cost for carbon emissions, representing the penalty incurred per ton of carbon dioxide emitted; e is the carbon emission factor, indicating the amount of carbon dioxide (in kilograms) emitted per kilowatt-hour of electricity generated; and $P_{loss,t}$ is the total active power loss of the network at time t.

The expression of F_{loss} is as follows:

$$F_{loss} = 365 \times \sum_{t=1}^{24} \sum_{i,j \in \Omega} I_{ij,t}^2 r_{ij} \Delta t \tag{10}$$

where Ω is the set of all branches of the distribution network; $I_{ij,t}$ is the current magnitude of branch ij at time t; r_{ij} is the resistance of branch ij.

3.3 Constraints

(1) Powe flow constraints:

$$u_{i,t} = U_{i,t}^2, u_{j,t} = U_{j,t}^2 \tag{11}$$

$$l_{ij,t} = I_{ij,t}^2 \tag{12}$$

$$u_{j,t} = u_{i,t} - 2\left(r_{ij}P_{ij,t} + x_{ij}Q_{ij,t}\right) + \left(r_{ij}^2 + x_{ij}^2\right) l_{ij,t} \tag{13}$$

$$\sum_{i:i \to j} \left(Q_{ij,t} - x_{ij} l_{ij,t}\right) - q_{j,t} = \sum_{k:j \to k} Q_{jk,t} \tag{14}$$

$$\sum_{i:i \to j} \left(P_{ij,t} - r_{ij} l_{ij,t}\right) - p_{j,t} = \sum_{k:j \to k} P_{jk,t} \tag{15}$$

$$u_{i,t} l_{ij,t} = P_{ij,t}^2 + Q_{ij,t}^2 \tag{16}$$

$$p_{j,t} = P_{load,j} - P_{j,t}^{DG} - P_{j,t}^{ESS} - P_{j,t}^{SOP} \tag{17}$$

$$q_{j,t} = Q_{load,j} - Q_{j,t}^{DG} - Q_{j,t}^{SOP} \tag{18}$$

where $j \to k$ indicates that node j is the upstream node of node k; $U_{i,t}$ and $U_{j,t}$ are the voltages of node i and node j at time t, respectively; $P_{jk,t}$ and $Q_{jk,t}$ represent the active and reactive power flowing from node j to node k at time t, respectively; $p_{j,t}$ and $q_{j,t}$ denote the net active and reactive loads at node j at time t, respectively; r_{ij} and x_{ij} are the resistance and reactance of the branch between nodes i and j; $P_{load,j}$ and $Q_{load,j}$ are the active and reactive load at node j, respectively; $P_{j,t}^{DG}$ and $Q_{j,t}^{DG}$ are the active and reactive power generated by the DG at node j at time t, respectively; $P_{j,t}^{ESS}$ is the charging/discharging power of the ESS installed at node j at time t, where positive values indicate discharging and negative values indicate charging; $P_{j,t}^{SOP}$ and $Q_{j,t}^{SOP}$ are the active and reactive power injected by the SOP to node j at time t.

Eq. (16) is nonlinear and nonconvex, but it can be reformulated into a standard second-order cone constraint through second-order cone relaxation:

$$\left\| \begin{matrix} 2P_{ij,t} \\ 2Q_{ij,t} \\ l_{ij,t} - u_{i,t} \end{matrix} \right\|_2 \leqslant l_{ij,t} + u_{i,t} \tag{19}$$

(2) Node voltage constraint:

$$u_{i,\min} \leq u_{i,t} \leq u_{i,\max} \tag{20}$$

where $u_{i,\min}$ and $u_{i,\max}$ denote the lower and upper bounds of the squared voltage magnitude at node i, respectively.

(3) Branch current constraint:

$$l_{ij,t} \leq l_{ij,\max} \tag{21}$$

where $l_{ij,\max}$ represents the upper bound of the squared current magnitude for branch ij.

(4) ESS operation constraints:

$$\begin{cases} \mu_{\mathrm{ch},i,t} + \mu_{\mathrm{dis},i,t} \leqslant 1 \\ \mu_{\mathrm{ch},i,t}, \mu_{\mathrm{dis},,t} \in \{0,1\} \end{cases} \tag{22}$$

$$0 \leqslant P_{\mathrm{ch},i,t} \leqslant \mu_{\mathrm{ch},i,t} P_{\mathrm{ESS},i}^{\max} \tag{23}$$

$$0 \leqslant P_{\mathrm{dis},i,t} \leqslant \mu_{\mathrm{dis},i,t} P_{\mathrm{ess},i}^{\max} \tag{24}$$

$$P_{i,t}^{\mathrm{ESS}} = P_{\mathrm{dis},i,t} - P_{\mathrm{ch},i,t} \tag{25}$$

$$\begin{cases} E_{\mathrm{SOC}}^{\min} \leqslant \mathrm{SOC}_{i,t} \leqslant E_{\mathrm{SOC}}^{\max} \\ \mathrm{SOC}_{i,1} = \mathrm{SOC}_{i,24} \end{cases} \tag{26}$$

$$\mathrm{SOC}_{i,t+1} = \mathrm{SOC}_{i,t} + \eta_{\mathrm{ch}} P_{\mathrm{ch},i,t} - \frac{1}{\eta_{\mathrm{dis}}} P_{\mathrm{dis},i,t} \tag{27}$$

where $\mu_{\mathrm{ch},i,t}$ and $\mu_{\mathrm{dis},i,t}$ are binary variables representing the charging and discharging states of the ESS at node i at time t; $\mu_{\mathrm{ch},i,t}$ and $\mu_{\mathrm{dis},i,t}$ are the charging and discharging efficiencies of the ESS, respectively; $P_{\mathrm{ESS},i}^{\max}$ is the maximum charging/discharging power of the ESS at node i at time t; $\mathrm{SOC}_{i,t}$ denotes the state of charge (SOC) of the ESS at time t; $E_{\mathrm{SOC}}^{\min}$ and $E_{\mathrm{SOC}}^{\max}$ are the minimum and maximum allowable SOC levels, respectively.

(5) SOP operation constraints:

$$\begin{cases} P_{i,t}^{\mathrm{SOP}} + P_{j,t}^{\mathrm{SOP}} + P_{ij,t}^{\mathrm{SOP}} = 0 \\ P_{ij,t}^{\mathrm{SOP}} = A_{i,\mathrm{SOP}} |P_{i,t}^{\mathrm{SOP}}| + A_{j,\mathrm{SOP}} |P_{j,t}^{\mathrm{SOP}}| \\ \left(P_{i,t}^{\mathrm{SOP}}\right)^2 + \left(Q_{i,t}^{\mathrm{SOP}}\right)^2 \leq \left(S_i^{\mathrm{SOP}}\right)^2 \\ \left(P_{j,t}^{\mathrm{SOP}}\right)^2 + \left(Q_{j,t}^{\mathrm{SOP}}\right)^2 \leq \left(S_j^{\mathrm{SOP}}\right)^2 \end{cases} \tag{28}$$

where $P_{ij,t}^{\mathrm{SOP}}$ is the transmission loss of the SOP between nodes i and j at time t; $A_{i,\mathrm{SOP}}$ and $A_{j,\mathrm{SOP}}$ are the loss coefficients of the two SOP converters, respectively; S_i^{SOP} and S_j^{SOP} are their corresponding installed capacities.

4 Case Study

In this paper, the IEEE 33-bus distribution system is used as a case study. First, the vulnerabilities of the 32 branches are evaluated using the Monte Carlo random sampling method. Then, nodes corresponding to low-vulnerability branches are selected as candidate locations for DG and ESS installation. Finally, the optimal installation locations and capacities of DG and ESS are determined within the candidate set by solving the proposed optimization model, which aims to minimize the annual comprehensive investment cost and network losses.

4.1 Parameter Settings

The IEEE 33-bus distribution system is adopted for analysis and validation, as illustrated in Fig. 2. The system operates at a voltage level of 12.66 kV, with an allowable voltage range of [0.95, 1.05] p.u. Detailed information on branch impedance and load power is available in [21]. Two dual-port SOPs are configured between nodes 12–22 and 18–33, respectively. Each SOP has a loss coefficient of 0.02. The rated output power of the ports at nodes 12 and 22 is 0.002 MVA, while that of the ports at nodes 18 and 33 is 0.01 MVA [22].

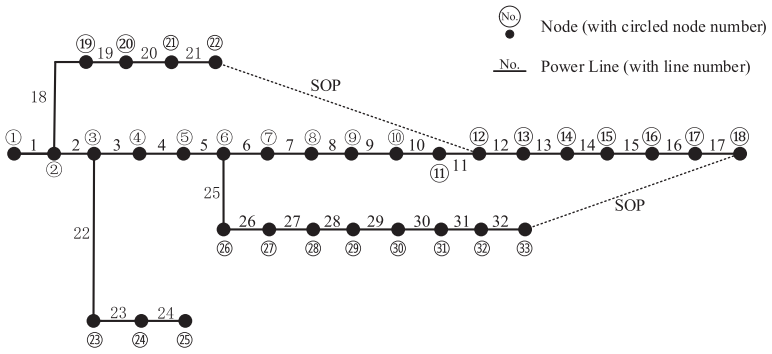

Figure 2: Topology of the IEEE 33-bus distribution system

The specific probabilities associated with different terrain-climate combinations, as referenced in Table 1, are detailed in Table 3.

Table 3: Specific probabilistic distribution of 12 climate-terrain condition combinations in the distribution network

State	Terrain	Climate	Probability
1	1	c	0.39
2	2	c	0.15
3	3	c	0.09
4	4	c	0.08
5	1	b	0.085
6	2	b	0.077
7	3	b	0.01
8	4	b	0.012
9	1	a	0.019
10	2	a	0.11
11	3	a	0.09
12	4	a	0.04

The service life of DG is assumed to be 20 years, with a fixed annual interest rate of 0.1. The investment cost is $500/kVA, and the annual operating cost is $70/kVA. For ESS, the service life is set at 15 years, with the same fixed annual interest rate of 0.1. The investment cost is $226.38/kW, and the annual operating cost is $175/kW [23].

Time-of-use electricity prices are listed in Table 4 [24], and the output coefficients of DG at each time interval are illustrated in Fig. 3.

Table 4: Time-of-use electricity price

Time interval	Type	Electricity price ($ /kW·h)
1–8	Valley Time	0.041
9, 15–19, 24	Usual Time	0.082
10–14, 20–23	Peak Time	0.12

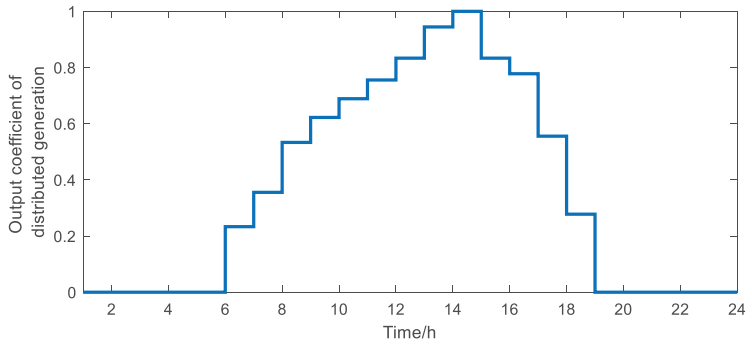

Figure 3: Output coefficients of DG over time

4.2 Vulnerability Calculation of Distribution Lines

The vulnerability indices of all 32 distribution lines are obtained from the Monte Carlo simulation results, as shown in Fig. 4. According to the law of large numbers, a larger number of sampling trials M yields probability estimates that more closely approximate their true values. Therefore, in this study, M = 100,000 is selected to ensure sufficient statistical stability of the Monte Carlo simulation results.

A lower vulnerability index represents a lower risk of lightning-induced failures. To ensure reliability in DG and ESS deployment, lines with vulnerability index values not exceeding 0.05 are selected as feasible installation candidates. A total of 24 lines meet this criterion, corresponding to Nodes 4, 6–9, 11–17, 19–21, 23, 24, and 26–32, which form the candidate set for the subsequent optimization.

4.3 Optimal Planning Results for DG and ESS Deployment

The optimal configuration model is solved using the CPLEX solver, resulting in the DG and ESS allocation scheme presented in Table 5.

The economic performance of the proposed configuration scheme is summarized in Table 6, with a total cost of $2,669,400.

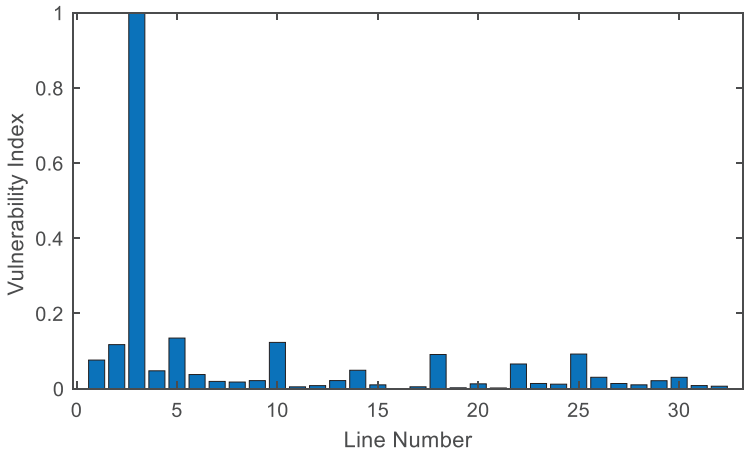

Figure 4: Line vulnerability index considering extreme weather based on Monte Carlo sampling

Table 5: Optimized configuration scheme of DG and ESS

Device type	Installation node number	Capacity
DG	19	0.42 MVA
ESS	29	0.5 MWh

Table 6: Economic indicators of the proposed configuration scheme

Objective function	Value ($ $\times 10^4$)
Annual investment and operating costs of DG	5.42
Annual investment and operating costs of ESS	10.24
Cost of purchasing power from the main grid	235.72
Cost of carbon emissions	15.56

Additionally, the annual network losses amount to 455.76 MWh. The hourly distribution of daily network losses is illustrated in Fig. 5.

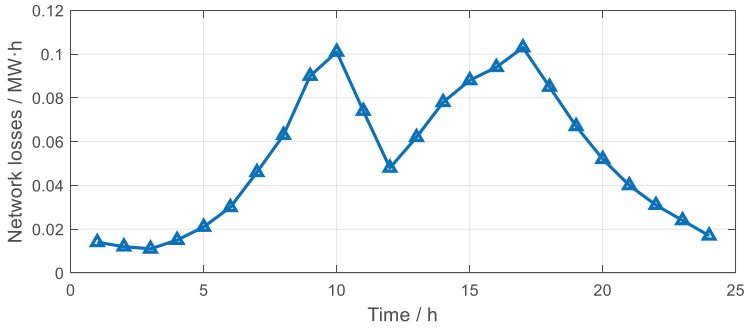

Figure 5: Hourly network loss over a single day

With the integration of DG and ESS, the voltage levels at each node are shown in Fig. 6. All node voltages remain within the specified limits.

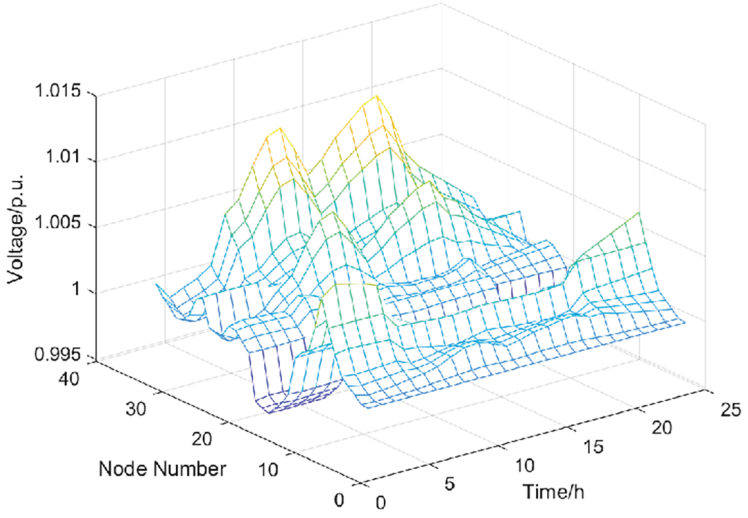

Figure 6: Daily voltage profile of each node

The 24-h charging and discharging profile of the ESS is illustrated in Fig. 7. During Periods 1–6, the ESS charges, taking advantage of low-load intervals to gradually increase the SOC. Subsequently, in Periods 7–9, the ESS remains idle, maintaining a stable SOC while avoiding unnecessary cycling. From Periods 10–14, the system enters a high-demand stage, and the ESS discharges to support network load and reduce grid power purchases. After this stage, the ESS briefly returns to charging in Periods 15–18 to restore part of its stored energy. During the later peak demand from Periods 20–23, the ESS discharges again to compensate for the shortage of local supply and mitigate peak load stress on the distribution network. Finally, the ESS returns to the idle state in Period 24. Overall, the schedule effectively achieves peak shaving and valley filling while maintaining feasible SOC operation throughout the day.

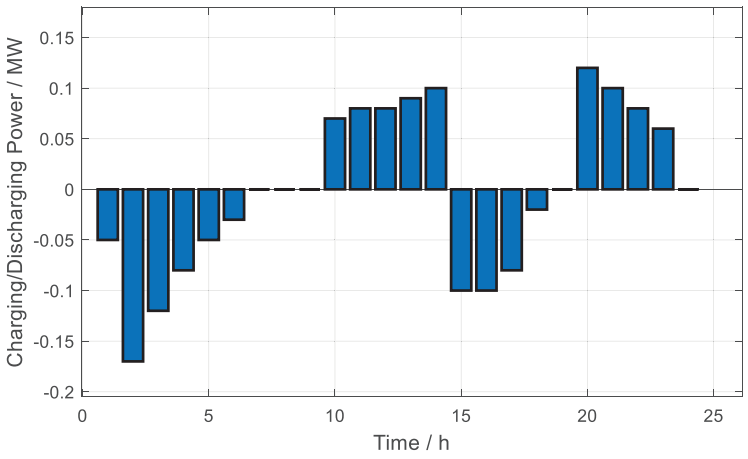

Figure 7: Daily charging and discharging power profile of the ESS

4.4 Necessity of Considering Line Vulnerability in DG and ESS Planning

To further demonstrate the necessity of incorporating line vulnerability into planning decisions, a benchmark DG-ESS planning model [25] is adopted for comparison. The benchmark approach optimizes DG and ESS solely based on economic operation and voltage constraints, without considering the increased failure risk of distribution lines under extreme weather conditions.

There are four planning strategies designed to quantitatively reflect how line vulnerability influences DG-ESS allocation decisions and overall distribution network performance.

- Case 1.1: DG and ESS are planned using the proposed vulnerability-aware methodology, where climate-induced line vulnerability is explicitly incorporated into the decision process.
- Case 1.2: Only DG is deployed using the proposed vulnerability-aware methodology, while ESS is not included.
- Case 2.1: DG and ESS are planned using the benchmark model [25], which focuses solely on economic performance and steady-state voltage constraints, without modeling line vulnerability.
- Case 2.2: Only DG is deployed using the benchmark model [25], while ESS and line vulnerability considerations are both excluded.

All four cases are applied to the IEEE 33-bus test system. The key metrics include annual total cost, annual network losses, average outage duration considering climate-adjusted line failure rate, and maximum node voltage deviation.

The comparison results are presented in Table 7. Firstly, the effectiveness of ESS can be evaluated by comparing Case 1.1 with Case 1.2 and Case 2.1 with Case 2.2. In both planning methods, including ESS significantly enhances system performance. For the proposed method, ESS deployment reduces the average outage duration by 21.66%, decreases annual network losses by 9.91%, and improves voltage regulation by 65.71%, at the expense of a modest cost increase of 4.87%. A similar pattern appears in the benchmark method, where ESS lowers the outage duration by 19.23%, cuts network losses by 10.56%, and reduces voltage deviation by 65.36%, with only a 4.92% increase in annual cost. These results indicate that ESS provides fast-response power support during contingencies and performs peak shaving and valley filling during normal operation. Therefore, the investment in ESS, despite slightly higher costs, is economically justified because the gains in operational flexibility, voltage quality, and supply continuity substantially outweigh the marginal increase in annual cost.

Table 7: Comparison of planning cases in cost and reliability

Metric	Case 1.1	Case 1.2	Case 2.1	Case 2.2
DG installation node number	19	11	18	18
DG capacity (MVA)	0.42	0.45	0.4	0.48
ESS installation node number	29	–	24	–
ESS capacity (MWh)	0.5	–	0.5	–
Annual total cost ($ $\times 10^4$)	266.94	254.55	269.52	256.87
Annual network losses (MWh)	455.76	505.91	453.62	507.15
Average outage duration (Hours/Year)	9.73	12.42	17.81	22.05
Max node voltage deviation (p.u.)	0.0119	0.0347	0.0124	0.0358
Computation time (s)	13.24	11.13	12.42	10.64

Then, the impact of incorporating line vulnerability can be evaluated by comparing Case 1.1 with Case 2.1 and Case 1.2 with Case 2.2. When DG and ESS are jointly planned, the vulnerability-aware strategy reduces the average outage duration by 45.37% compared with the benchmark method, while maintaining slightly lower annual cost and voltage deviation and keeping network losses nearly unchanged. Even for DG-only planning, considering line vulnerability still shortens the outage duration by 43.67%. These results demonstrate that proactively avoiding vulnerable lines enables more resilient resource allocation, prevents substantial performance degradation under weather-induced contingencies, and significantly enhances the distribution network's ability to withstand climate-driven uncertainties.

Besides, to examine whether the preceding Monte Carlo-based vulnerability evaluation increases computational burden, the computation time of each case is also analyzed. The results show that the total computation time of Case 1.1 and Case 1.2, which includes the Monte Carlo simulation performed in the preprocessing stage, remains comparable to that of the benchmark cases. This indicates that the additional vulnerability assessment introduces negligible computational overhead while improving the robustness of planning decisions.

In summary, ESS contributes to operational flexibility and enhanced reliability, while vulnerability-aware planning ensures robust resource placement. The combination of the two features in Case 1.1 achieves the best performance in terms of cost-resilience balance, clearly demonstrating the superiority and practical necessity of the proposed planning approach.

5 Conclusions

This paper proposes a comprehensive optimization framework for the coordinated allocation of DG and ESS, explicitly incorporating line vulnerability under extreme weather conditions. A Monte Carlo-based vulnerability assessment is developed to quantify the impact of micro-climatic and terrain factors on line failure risk, providing a data-driven foundation for resilient resource siting. Building on this assessment, a multi-objective optimization model is formulated to minimize annual investment, operation, and maintenance costs, as well as network losses, while satisfying technical and operational constraints. Application to the IEEE 33-bus distribution system demonstrates that the proposed method significantly enhances system resilience and operational flexibility, achieving lower outage duration and voltage deviation with minimal cost increase.

The key methodological contribution lies in integrating vulnerability evaluation into DG and ESS planning, thereby bridging economic optimization with resilience-oriented decision-making. The results confirm that proactively avoiding high-risk lines and strategically deploying ESS can yield a cost-effective and resilient network configuration.

Overall, the proposed framework provides a practical and scalable approach for enhancing both the economy and resilience of DG and ESS planning in distribution networks. Future research will extend the framework to more complex operational environments, accounting for correlated weather uncertainties and investment risks. Furthermore, the proposed planning methodology could be integrated into virtual power plant frameworks to support aggregated operation and resilience-oriented coordination of DG and ESS [26,27].

Acknowledgement: Not applicable.

Funding Statement: This paper is supported by the Science and Technology Project of Southern Power Grid Guangxi Power Grid Co., Ltd. (GXKJXM20222157).

Author Contributions: The authors confirm contribution to the paper as follows: study conception and design: Yangjun Zhou, Juntao Pan; data collection: Chenying Yi, Weixiang Huang, Like Gao, Shan Li, Liwen Qin; analysis and interpretation of results: Yangjun Zhou, Shan Li; methodology development: Yangjun Zhou, Wei Zhang; draft manuscript preparation: Yangjun Zhou; manuscript review and editing: Juntao Pan, Ke Zhou, Ling Li, Lijuan Yan; funding acquisition: Juntao Pan, Yuanchao Zhou, Hongwen Wu. All authors reviewed the results and approved the final version of the manuscript.

Availability of Data and Materials: Data supporting this study are included within the article.

Ethics Approval: Not applicable.

Conflicts of Interest: The authors declare no conflicts of interest to report regarding the present study.

Glossary

DG	Distributed Generation
ESS	Energy Storage System
SOP	Soft Open Point

References

1. Rifkin J. The third industrial revolution: how lateral power is transforming energy, the economy, and the world. New York, NY, USA: Palgrave Macmillan; 2011. p. 17–9.
2. Zhao S, Shao C, Ding J, Hu B, Xie K, Yu X, et al. Unreliability tracing of power systems for identifying the most critical risk factors considering mixed uncertainties in wind power output. Prot Control Mod Power Syst. 2024;9(5):96–111. doi:10.23919/PCMP.2023.000022.
3. Xu L, Hu B, Shao C, Xie K, Pan C, Tai H-M, et al. A fully analytical approach for the real-time dynamic reliability evaluation of composite power systems with renewable energy sources. Engineering. 2025;51(3):144–57. doi:10.1016/j.eng.2024.09.023.
4. Koutsoukis NC, Siagkas DO, Georgilakis PS, Hatziargyriou ND. Online reconfiguration of active distribution networks for maximum integration of distributed generation. IEEE Trans Autom Sci Eng. 2017;14(2):437–48. doi:10.1109/TASE.2016.2628091.
5. Singh M, Khadkikar V, Chandra A, Varma RK. Grid interconnection of renewable energy sources at the distribution level with power-quality improvement features. IEEE Trans Power Deliv. 2011;26(1):307–15. doi:10.1109/TPWRD.2010.2081384.
6. Yang X, Xu C, Zhang Y, Yao W, Wen J, Cheng S. Real-time coordinated scheduling for ADNs with soft open points and charging stations. IEEE Trans Power Syst. 2021;36(6):5486–99. doi:10.1109/TPWRS.2021.3070036.
7. Gao Y, Hu X, Yang W, Liang H, Li P. Multi-objective bilevel coordinated planning of distributed generation and distribution network frame based on multiscenario technique considering timing characteristics. IEEE Trans Sustain Energy. 2017;8(4):1415–29. doi:10.1109/TSTE.2017.2680462.
8. Al-Ja'Afreh MAA, Amjad B, Rowe K, Mokryani G, Angarita Marquez JL. Optimal planning and forecasting of active distribution networks using a multi-stage deep learning based technique. Energy Rep. 2023;10(14):686–705. doi:10.1016/j.egyr.2023.07.014.
9. Li Q, Chen J, Yang J, Li Z. Research on source network load–storage hierarchical coordinated intelligent control method for active distribution network. Electr Eng. 2025;107(1):1191–202. doi:10.1007/s00202-024-02524-3.
10. Lee SJ, Kim JH, Kim CH, Kim SK, Kim ES, Kim DU, et al. Coordinated control algorithm for distributed battery energy storage systems for mitigating voltage and frequency deviations. IEEE Trans Smart Grid. 2016;7(3):1713–22. doi:10.1109/TSG.2015.2429919.
11. Moghaddam IN, Chowdhury BH, Mohajeryami S. Predictive operation and optimal sizing of battery energy storage with high wind energy penetration. IEEE Trans Ind Electron. 2018;65(8):6686–95. doi:10.1109/TIE.2017.2774732.

12. Wang X, Yue M, Muljadi E, Gao W. Probabilistic approach for power capacity specification of wind energy storage systems. IEEE Trans Ind Appl. 2014;50(2):1215–24. doi:10.1109/TIA.2013.2272753.
13. Luo F, Meng K, Dong ZY, Zheng Y, Chen Y, Wong KP. Coordinated operational planning for wind farm with battery energy storage system. IEEE Trans Sustain Energy. 2015;6(1):253–62. doi:10.1109/TSTE.2014.2367550.
14. Wang Y, Lv B, Liu X, Yu F. Distribution network planning considering offshore wind–tide–virtual energy storage system. In: Proceedings of the IEEE International Electrical and Energy Conference(CIEEC); 2019 Sep 7–9; Beijing, China. p. 886–9. doi:10.1109/CIEEC47146.2019.CIEEC-2019341.
15. Atwa YM, El-Saadany EF. Optimal allocation of ESS in distribution systems with a high penetration of wind energy. IEEE Trans Power Syst. 2010;25(4):1815–22. doi:10.1109/TPWRS.2010.2045663.
16. Wen S, Lan H, Fu Q, Yu DC, Zhang L. Economic allocation for energy storage system considering wind power distribution. IEEE Trans Power Syst. 2015;30(2):644–52. doi:10.1109/TPWRS.2014.2337936.
17. Ravichandran N, Proto D, Mottola F, Andreotti A. Multi-objective optimization for lightning protection in distribution networks: a novel approach based on design of experiments. IEEE Access. 2025;13(3):45215–26. doi:10.1109/ACCESS.2025.3546490.
18. Kinney R, Crucitti P, Albert R, Latora V. Modeling cascading failures in the North American power grid. Eur Phys J B. 2005;46(1):101–7. doi:10.1140/epjb/e2005-00237-9.
19. Jiang X, Xiang Z, Zhang Z, Hu J, Hu Q, Shu L. Predictive model for equivalent ice thickness load on overhead transmission lines based on measured insulator string deviations. IEEE Trans Power Deliv. 2014;29(4):1659–65. doi:10.1109/TPWRD.2014.2305980.
20. Khodadadi N, Khodadadi E, Abdollahzadeh B, Ei-Kenawy E-SM, Mardanpour P, Zhao W, et al. Multi-objective generalized normal distribution optimization: a novel algorithm for multi-objective problems. Clust Comput. 2024;27(8):10589–631. doi:10.1007/s10586-024-04467-7.
21. Baran ME, Wu FF. Network reconfiguration in distribution systems for loss reduction and load balancing. IEEE Trans Power Deliv. 1989;4(2):1401–7. doi:10.1109/61.25627.
22. Jiang L, Wang C, Qiu W, Xiao H, Hu W. A flexible interconnected distribution network power supply restoration method based on E-SOP. Energies. 2025;18(4):954. doi:10.3390/en18040954.
23. Zhao B, Xu Z, Xu C, Wang C, Lin F. Network partition-based zonal voltage control for distribution networks with distributed PV systems. IEEE Trans Smart Grid. 2018;9(5):4087–98. doi:10.1109/TSG.2017.2648779.
24. Zheng S, Sun Y, Qi B, Li B. Incentive-based integrated demand response considering S&C effect in demand side with incomplete information. IEEE Trans Smart Grid. 2022;13(6):4465–82. doi:10.1109/TSG.2022.3149959.
25. Li R, Chen B, Bai X. A bi-level model for DG and ESS integrated planning in distribution system. In: Proceedings of the IEEE Conference on Energy Internet and Energy System Integration(EI2); 2020 Oct 30–Nov 1; Wuhan, China. p. 2234–8. doi:10.1109/EI250167.2020.9347197.
26. Xiao D. A review on risk-averse bidding strategies for virtual power plants with uncertainties: resources, technologies, and future pathways. Technologies. 2025;13(11):488. doi:10.3390/technologies13110488.
27. Yu S, Fang F, Liu Y, Liu J. Uncertainties of virtual power plant: problems and countermeasures. Appl Energy. 2019;239(7):454–70. doi:10.1016/j.apenergy.2019.01.224.